JGR Oceans

RESEARCH ARTICLE
10.1029/2020JC017057

Seasonal and Mesoscale Variability of the Two Atlantic Water Recirculation Pathways in Fram Strait

Zerlina Hofmann[1], Wilken-Jon von Appen[1], and Claudia Wekerle[1,2]

[1]Physical Oceanography of the Polar Seas, Alfred Wegener Institute, Helmholtz Centre for Polar and Marine Research, Bremerhaven, Germany, [2]Climate Dynamics, Alfred Wegener Institute, Helmholtz Centre for Polar and Marine Research, Bremerhaven, Germany

Key Points:

- We present the first multi-year mooring-based observations of the Atlantic Water recirculation at the prime meridian
- At 78°50'N we observe a continuous westward flow, present throughout the year and most affected by eddies in spring
- At 80°10′N we only observe passing eddies, which are strongest during late autumn and winter, and absent during summer

Correspondence to:
Z. Hofmann,
zerlina.hofmann@awi.de

Citation:
Hofmann, Z., von Appen, W.-J., & Wekerle, C. (2021). Seasonal and mesoscale variability of the two Atlantic Water recirculation pathways in Fram Strait. *Journal of Geophysical Research: Oceans*, *126*, e2020JC017057. https://doi.org/10.1029/2020JC017057

Received 8 DEC 2020
Accepted 9 JUN 2021

Abstract Atlantic Water (AW), which is transported northward by the West Spitsbergen Current (WSC), partly recirculates (i.e., turns westward) in Fram Strait. This determines how much heat and salt reaches the Arctic Ocean, and how much joins the East Greenland Current on its southward path. We describe the AW recirculation's location, seasonality, and mesoscale variability by analyzing the first observations from moored instruments at five latitudes in central Fram Strait, spanning a period from August 2016 to July 2018. We observe recirculation on the prime meridian at 78°50'N and 80°10'N, respectively south and north of the Molloy Hole, and no recirculation further south at 78°10'N and further north at 80°50'N. At a fifth mooring location northwest of the Molloy Hole at 79°30'N, we observe some influence of the two recirculation pathways. The southern recirculation is observed as a continuous westward flow that carries AW throughout the year, though it may be subject to broadening and narrowing. It is affected by eddies in spring, likely due to the seasonality of mesoscale instability in the WSC. The northern recirculation is observed solely as passing eddies on the prime meridian, which are strongest during late autumn and winter, and absent during summer. This seasonality is likely affected both by the conditions set by the WSC and by the sea ice. Open ocean eddies originating from the WSC interact with the sea ice edge when they subduct below the fresher, colder water.

Plain Language Summary West of Spitsbergen, the so-called West Spitsbergen Current (WSC) carries relatively warm water towards the Arctic Ocean. Part of this water turns westward before it reaches the Arctic Ocean. Another current transports it back south along the Greenland shelf. We look at observations of temperature, salinity, and flow velocity from two years in the region. We find that the warm water flows westwards at two latitudes. At 78°50'N it flows westwards throughout the year, but is affected by eddies in the ocean during spring. These eddies also carry warm water westwards and likely originate from the WSC. At 80°10'N, the warm water passes only over periods of a few days, and only during late autumn, winter, and spring. That means that we do not observe the warm water flowing westwards at this latitude, but only eddies that carry it westwards. These eddies also originate from the WSC, and their properties likely change, when they meet the ice edge and have to push underneath.

1. Introduction

Fram Strait is the only deep connection (~2,500 m) between the Arctic Ocean and the Nordic Seas. Warm, saline water from the Atlantic Ocean enters via the West Spitsbergen Current (WSC) on the eastern side of the strait. Colder, fresher water and sea ice (as well as modified water, which was previously warm and saline) from the Arctic Ocean exits via the East Greenland Current (EGC) on the western side (Figure 1a). Part of the Atlantic Water (AW), however, recirculates (i.e., turns westward) in Fram Strait before reaching the Arctic Ocean. Recirculating AW significantly impacts the redistribution of oceanic heat between the Nordic Seas and the Arctic Ocean (Hattermann et al., 2016), ultimately determining how much of the heat, salt, and other tracers such as nutrients carried by the WSC reaches the Arctic Ocean and how much joins the EGC on its southward path.

Overall, the AW that flows into the Nordic Seas is one of the sources from which (albeit heavily modified) intermediate and deep waters are produced. These waters overflow across the Greenland-Scotland-Ridge and ultimately contribute to the lower limb of the Atlantic Meridional Overturning Circulation (Hansen & Østerhus, 2000). The AW recirculation in Fram Strait is the northernmost extent of the boundary current loop

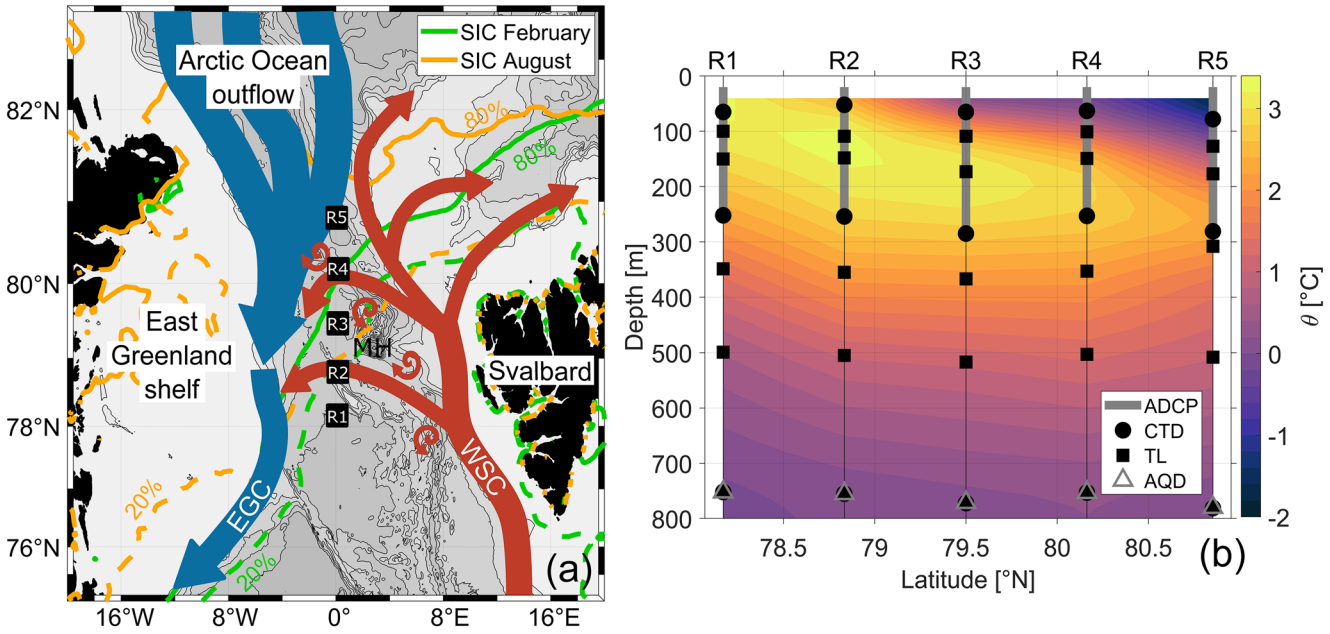

Figure 1. (a) Schematic circulation of Fram Strait with the West Spitsbergen Current (WSC) in red and the Arctic Ocean outflow and the East Greenland Current (EGC) in blue, with bathymetry from Schaffer et al. (2019), and the location of the Molloy Hole (MH). The black squares mark the location of moorings R1 through R5. Solid lines indicate the isoline of 80% sea ice concentration (SIC) in February (green) and August (orange), dashed lines indicate the isoline of 20% SIC during the same months, based on AMSR-E and AMSR2 measurements from 2003 to 2018. (b) Gridded potential temperature (°C) section, averaged over the entire period of the observations, with instrument locations in the water column. The gray bars mark the Acoustic Doppler Current Profilers (ADCP), the black dots the CTDs (measuring conductivity, temperature, and pressure, (giving depth)), the black squares the temperature loggers (TL), and the gray triangles the Aquadopps (AQD, measuring point velocity).

in the Nordic Seas (Mauritzen, 1996). As the AW subducts below the fresher, colder waters of the western Fram Strait, atmospheric modification is not possible downstream. By impacting hydrographic properties of waters transported into and out of the Arctic Ocean, the AW recirculation affects all known mechanisms of intermediate and deep water formation in the Arctic Ocean and the Greenland Sea (Mauritzen, 1996; Rudels & Quadfasel, 1991).

Previous observational efforts in central Fram Strait have shed some light on the existence and location of the recirculation. They include ship, ice camp, and float based measurements during the 1983/84 Marginal Ice Zone Experiment (e.g., Johannessen et al., 1987; Quadfasel et al., 1987), as well as CTD measurements (e.g., Manley, 1995; Marnela et al., 2013). These observations are, however, limited to synoptic summer-time observations. A mooring array that has been deployed across Fram Strait at 78°50'N since 1997 provides more long-term observations, but the analysis of the mooring data is limited to this one latitude and has been focused on the boundary currents (e.g., Beszczynska-Möller et al., 2012; de Steur et al., 2014). Furthermore, studies have addressed the potential generation mechanisms of the recirculation in the WSC (Crews et al., 2019; von Appen et al., 2016) and the contribution of the AW recirculation to the EGC (Håvik et al., 2017).

Inflow and outflow through Fram Strait via the boundary currents has been simulated with different model setups (e.g., Aksenov et al., 2010; Ilicak et al., 2016). Whether the resulting transports compare well to observations largely depends on whether the model achieves some representation of our limited current knowledge of the recirculation of AW in Fram Strait. However, the models remain inconclusive about the exact location and strength of individual recirculation pathways, the northern limit of the recirculation, and the strength of the boundary currents. One of the main issues is the resolution necessary to resolve mesoscale eddies that play a large role in the recirculation in Fram Strait (Gascard et al., 1988, 1995). The horizontal scale of these eddies is governed by the local internal Rossby radius of deformation (Fieg et al., 2010), which is about 2–6 km in the WSC (von Appen et al., 2016) and about 6 km in the EGC (Zhao et al., 2014). Only

more recent modeling efforts in Fram Strait can be considered eddy-resolving (e.g., Hattermann et al., 2016; Wekerle et al., 2017).

Both observational and model studies have suggested that the bulk of the recirculation occurs along two pathways between 78°N and 81°N (Figure 1a). One is located along the Spitsbergen Fracture Zone and south of the Molloy Hole (e.g., Gascard et al., 1995; Rudels et al., 2005; Wekerle et al., 2017). The other is located along the Molloy Fracture Zone and north of the Molloy Hole (e.g., Bourke et al., 1988; Hattermann et al., 2016; Quadfasel et al., 1987). There has been clear evidence of mesoscale eddies in the central Fram Strait (Rudels et al., 2005), which are likely generated along the continental slope off Spitsbergen in the WSC (Gascard et al., 1988, 1995), as well as highly energetic motions on smaller scales, i.e., at the submesoscale (Bashmachnikov et al., 2020; von Appen et al., 2018). Instead of a continuous stream, the recirculation may solely exist as westward propagating WSC eddies (Gascard et al., 1988; Rudels et al., 2005), though these may be advected by a background flow (Johannessen et al., 1987).

While previous studies mostly agree on the fraction of AW that recirculates, which is considered half of the AW entering Fram Strait (de Steur et al., 2014; Marnela et al., 2013; Rudels, 1987), this has been suggested to vary between seasons. Hattermann et al. (2016) differentiate between 60% recirculation in late winter/spring and 30% recirculation in summer (when the total AW inflow to Fram Strait is also weaker). Observations by von Appen et al. (2016) indicate that the recirculation likely advects eddies across Fram Strait during winter and spring, with a peak in observed eddy kinetic energy (EKE) in the WSC during January–February and in central Fram Strait 1–2 months later. During summer, observed EKE is generally much smaller. Modeling studies also find the highest values of EKE in the WSC, and export of water westwards, to be the strongest during winter (Hattermann et al., 2016; Wekerle et al., 2017). Wekerle et al. (2017) did not find all recirculation pathways to be present during summer, when the circulation north of the Molloy Hole was absent.

In this study, we aim to narrow down the location of the AW recirculation, present direct observations of its seasonality, and gather a better understanding of its mesoscale variability. We analyze the first long-term hydrographic observations of the AW recirculation at multiple latitudes in central Fram Strait, as well as output from an eddy-resolving sea ice-ocean model. The results of this study add to our knowledge of the AW recirculation, including its dynamical understanding.

2. Data and Methods

2.1. Meridional Mooring Array

During cruise PS100 of RV Polarstern in July/August 2016, five equally spaced moorings with a distance of ~75 km or 40' of latitude in between them were deployed along the prime meridian in Fram Strait (Figure 1a). They measured temperature, salinity, oxygen, and velocity in the upper 800 m of the water column (Kanzow, 2017). All moorings were successfully recovered during cruise PS114 in July/August 2018 (von Appen, 2018). They are archived as moorings R1-1 at 78°10'N/00°00'E, R2-1 at 78°50'N/00°00'E, R3-1 at 79°30'N/00°00'E, R4-1 at 80°10'N/00°10'E, and R5-1 at 80°50'N/00°07'W. The moorings were in water depths from 2,597 to 3,140 m. From here on we will refer to them as R1 through R5, with R1 being the southernmost mooring at 78°10'N, and R5 being the northernmost mooring at 80°50'N. Data are available on PANGAEA (von Appen, 2019).

The instruments recovered from the moorings relevant to this work are SeaBird SBE37 CTDs with an oxygen sensor, measuring temperature, conductivity, pressure, and oxygen; SeaBird SBE56 temperature loggers (TL), measuring temperature; RDI 150 kHz Acoustic Doppler Current Profilers (ADCPs), measuring velocity profiles, temperature, and pressure; and NORTEK Aquadopps for deep water, measuring point velocity, and temperature. The locations of the instruments in the water column are marked in Figure 1b.

As all instruments recorded at least every hour, we applied a low-pass filter at a period of 1 h to all the time series of instruments that recorded more often (i.e., the TL that recorded every 30 s, and the Aquadopps that recorded every 20 min). We then interpolated the data of each mooring with a minimum curvature gridding method with an added tension parameter (Smith & Wessel, 1990). The resulting data set has a temporal resolution of 1 h (i.e., the time step of the filtered measurements) and a vertical resolution of 20 m.

The grid extends over a time period from August 10, 2016 to July 19, 2018 (as this is the period covered by all instruments, i.e., the date of the last mooring deployment to the date of the first mooring recovery) and over a depth from 40 m (20 m for velocity measurements) to 1,100 m. This way, we excluded no measurements. The instruments furthest down in the water column only had a target depth of 750–780 m; however, at times the moorings were subjected to strong motion that deepened the instruments, and we included measurements acquired during those times in the interpolation. For analysis, we then removed the gridded data below 800 m.

Except for a few individual missing measurements, only three of the CTDs malfunctioned for more than a month each. We replaced missing temperature and pressure measurements with nearby ADCP measurements. We calculated missing salinity measurements from temperature measurements, where we determined the relationship between the two by a linear regression with the data that was available at the instrument. The ADCPs measured velocity profiles with 70 bins, of which ~8% were lost toward the surface, which translates roughly to the upper 20 m. The TL recorded without any issues and we excluded no data. Further information on data processing and handling of missing data can be found in Hofmann (2020).

2.2. Zonal Mooring Array

At the latitude of R2 (78°50'N) a longer time series of the existing mooring array covering the zonal extent of Fram Strait was available. The closest mooring was F16, which was in the water from August 2002 to September 2014 and located 9 km east of 0°EW. We used it to validate the observations at R2. Data are available on PANGAEA (von Appen et al., 2019).

2.3. Sea Ice Concentration

Sea ice concentration data were taken from the Advanced Microwave Scanning Radiometers AMSR-E and AMSR2 (Spreen et al., 2008) and evaluated for individual moorings by choosing the nearest grid point to the mooring position. Data are available on PANGAEA (Melsheimer & Spreen, 2019, 2020).

2.4. Ocean-Sea Ice Model

In this study, we used model data from the Finite-Element Sea ice-Ocean Model (FESOM) version 1.4 (Wang et al., 2014). FESOM is a sea ice-ocean model that solves the hydrostatic primitive equations for the ocean and comprises a finite element sea ice component. It uses triangular surface meshes for spatial discretization, allowing for a refined mesh in regions of interest, while keeping a coarser mesh elsewhere.

In the model configuration used here, a mesh resolution of nominally 1° was applied in the global oceans. The mesh was refined to 25 km north of 40°N, and to 4.5 km in the Nordic Seas and Arctic Ocean. In the wider Fram Strait (20°W–20°E/76°N–82°30'N), the mesh was further refined to 1 km. In this region, the simulation can be considered as eddy-resolving, as the local internal Rossby radius of deformation is about 2–6 km (von Appen et al., 2016; Zhao et al., 2014). In the vertical, the model used 47 z-levels with a resolution of 10 m in the upper 100 m, and coarser resolution with depth (with a resolution of ~100 m at 800 m depth). For bottom topography, the RTopo-2 data set was used (Schaffer et al., 2016). The model simulation covers the period 2010–2018 and has daily model output. It was forced with atmospheric reanalysis data from ERA-Interim (Dee et al., 2011), and was initialized with model fields from the simulation described in Wekerle et al. (2017). River runoff (except for Greenland) was taken from the JRA-55 data set (Tsujino et al., 2018), and Greenland ice-sheet runoff was taken from Bamber et al. (2018). Tides were not included in this simulation. Here we studied the model data of August 2016 to July 2018 at 0°EW in Fram Strait for comparison with our observations. Model output are available on Zenodo (Wekerle, 2021).

2.5. Derived Variables

We calculated both potential temperature θ and potential density Σ_0 with the SeaWater library of EOS-80 (Nayar et al., 2016; Sharqawy et al., 2010) from gridded salinity, temperature, and pressure, with a reference

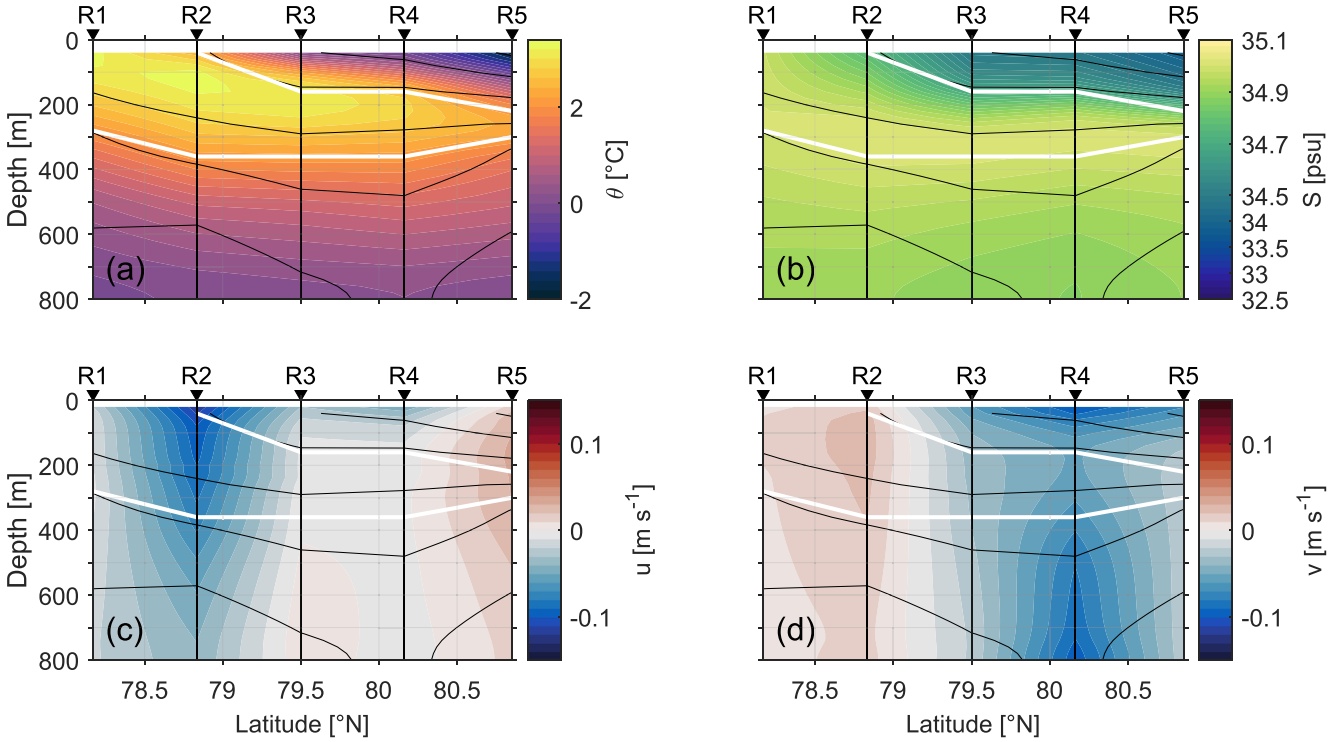

Figure 2. Gridded sections of (a) potential temperature (°C), (b) salinity (psu), (c) zonal velocity (m s^{-1}), and (d) meridional velocity (m s^{-1}), averaged over the entire time series. Note the nonlinear color bar of salinity. The black lines mark the 27.3, 27.5, 27.7, 27.9, 27.95, and 28 kg m^{-3} isopycnals. The white lines mark the lower and upper boundary of the Atlantic Water (AW) layer. While the interpolated data display might suggest otherwise, our information stems only from the five mooring locations and we cannot speculate about conditions between moorings.

pressure of zero. To evaluate the EKE associated with the mesoscale variability, we bandpass filtered the velocity data between 2 and 30 days (as done in von Appen et al., 2016), and used the filtered u', v' to evaluate

$$\mathrm{EKE} = \frac{1}{2} \cdot [u'^2 + v'^2]. \tag{1}$$

The short period limit avoids tides and inertial oscillations and the long period limit removes the seasonal cycle and interannual variations of the velocities. Additionally we determined the relative importance of EKE by calculating mean kinetic energy (MKE) from time-averaged velocities $\overline{u}, \overline{v}$ as follows:

$$\mathrm{MKE} = \frac{1}{2} \cdot [\overline{u}^2 + \overline{v}^2]. \tag{2}$$

For all variables, we calculated monthly averages, i.e., we averaged over all measurements from each of the 24 months of measurements (August 2016 to July 2018). The monthly averages of August 2016 and July 2018 were based on fewer measurements than for other months because the measurements only started in mid-August 2016 and ended in mid-July 2018. We did the monthly averaging for each of the five moorings and each of the 40 depth levels individually. For monthly averages of the full vertical extent of the grid, we then averaged the monthly averages over the 40 depth levels.

3. Mean State of the Two Atlantic Water Recirculation Pathways

On average over the full two-year time series, we observe a layer of water with relatively high potential temperature and salinity at 0°EW in central Fram Strait. This water fits the AW definition, here defined as water with a potential density $27.7 < \sigma_0 \leq 27.97$ kg m^{-3} and a potential temperature $\theta > 2$°C after the definition of AW outside the WSC by Rudels et al. (2005). The AW is located at the surface at the southernmost moor-

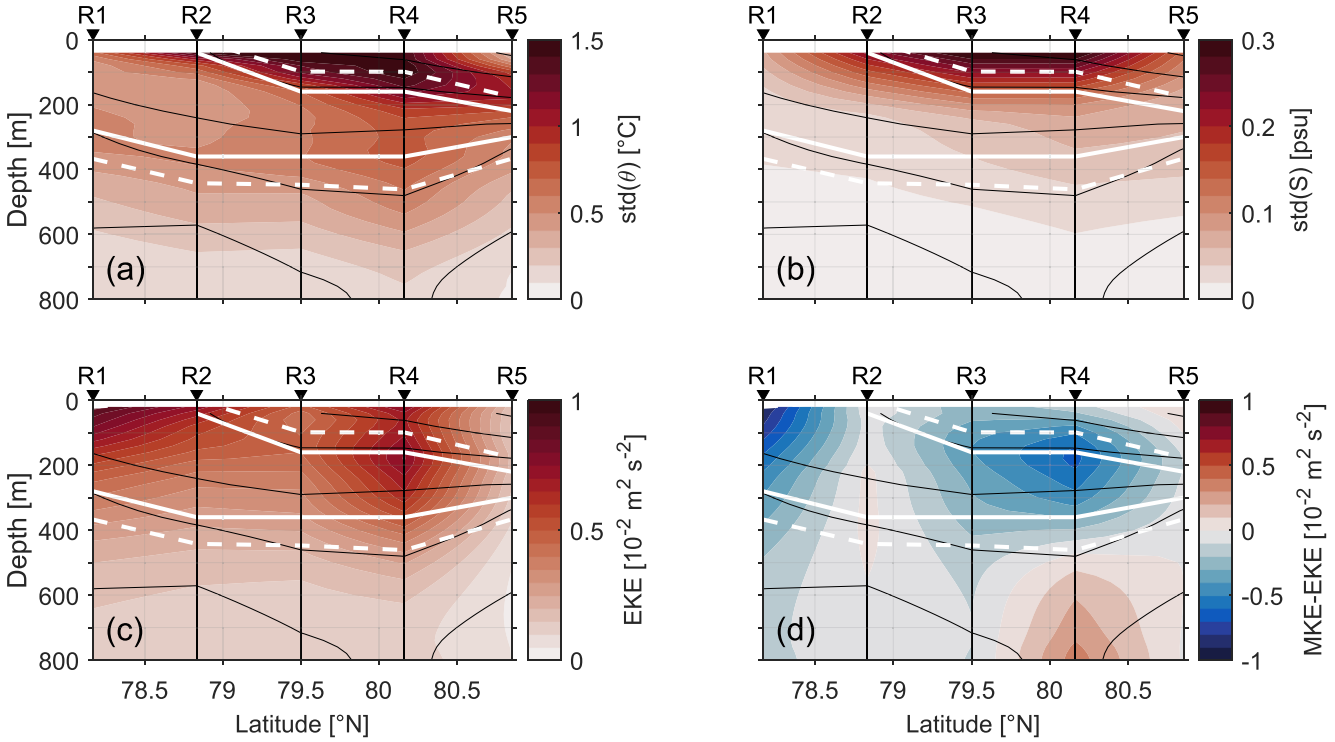

Figure 3. Gridded sections of (a) the standard deviation of potential temperature (°C), (b) the standard deviation of salinity (psu), (c) eddy kinetic energy (EKE) ($m^2\ s^{-2}$), and (d) mean kinetic energy (MKE) minus EKE ($m^2\ s^{-2}$), averaged over the entire time series. The black lines mark the 27.3, 27.5, 27.7, 27.9, 27.95, and 28 kg m^{-3} isopycnals. The solid white lines mark the mean lower and upper boundary of the Atlantic Water (AW) layer. The dashed white lines mark the lower boundary of the AW layer plus one standard deviation of the lower boundary depth and the upper boundary of the AW layer minus one standard deviation of the upper boundary depth. While the interpolated data display might suggest otherwise, our information stems only from the five mooring locations and we cannot speculate about conditions between moorings.

ing R1 (78°10'N) and progressively further down in the water column, thinning toward the north, where it is covered by colder, less saline water (Figure 2a and 2b). This is due to a growing influence of sea ice on surface waters with increasing latitude. R1 is the only mooring location largely unaffected by sea ice, while the ice cover at the moorings further north increases with latitude; the northernmost is mostly ice covered throughout the year (Figure 1a). We consider different parameters to be indicative of AW recirculation at 0°EW. These include comparatively high potential temperature, salinity, and AW layer thickness, strong westward velocities, and high EKE.

We observe high potential temperature, salinity, potential density, and AW layer thickness at the southernmost mooring R1 (Figure 2a and 2b), but no westward flow (Figure 2c). While there is a strong EKE maximum close to the surface at R1 (Figure 3c), this is not accompanied by strong variations in potential temperature or salinity (Figure 3a and 3b) and thus likely not associated with recirculating AW. Note that our observations are Eulerian at a constant depth. Passing mesoscale eddies which are in geostrophic balance would be associated with sloping isopycnals (and thus sloping isotherms and isohalines) that would be advected past the moored observation point. Therefore, eddies with AW in their core would lead to variability in temperature and salinity, although the effect might be weaker if the ambient water outside of the eddies was also AW compared to other water masses. At the northernmost mooring R5 (80°50'N, west of the Yermak Plateau) we observe little AW, low surface densities, and no other indicators of recirculation (Figure 2). We infer, therefore, that the bulk of the recirculation occurs between R1 and R5. At the central mooring R3 (79°30'N) we observe a similar mean state as further north, but with a weaker southward flow (Figure 2), as well as little EKE and variability in potential temperature and salinity (Figure 3). The Arctic Ocean outflow likely transports some AW from the north toward this location, but the lack of variability in AW properties on mesoscale time scales or westward flow gives little indication for recirculation occurring at this latitude. However, monthly averages reveal a maximum in potential temperature, salinity, AW layer thickness, and

EKE in April 2017 (not shown), which could indicate some influence from the south. While the situation at 79°30'N is certainly interesting, analysis of the times during which it is influenced by recirculation are beyond the scope of this study and would benefit from a longer period of observations.

We will hence focus our analysis on R2 and R4. Note that the 75 km horizontal resolution of the mooring array cannot resolve submesoscale or even mesoscale dynamics in this region, which are rather important for the recirculation. While the interpolated data display (Figures 2 and 3) might suggest otherwise, our information stems only from the five mooring locations and we cannot speculate about conditions between moorings. Still, the mooring locations were chosen with purpose. R2 and R4 are located along the Spitsbergen Fracture Zone and the Molloy Fracture Zone, respectively. Previous studies have suggested that recirculation in that region may be related to the steep bathymetric slopes. The added equidistant moorings south, in between, and north of R2 and R4 give us an indication of the width of the recirculation so that we are able to narrow down the location of the recirculation pathways and add to a better understanding of their variability. Based on different properties, we can identify two AW recirculation pathways at R2 and R4.

3.1. Southern Recirculation (R2)

The maxima of both mean potential temperature and mean salinity are found at R2 (78°50'N), where the mean AW layer thickness is also largest (Figure 2a and 2b). This is accompanied by strong westward (and slightly northward) velocities, indicating (north-)westward moving AW, i.e., recirculation (Figure 2c and 2d). The observed signal at R2 varies little in potential temperature and salinity, and as these two variables determine potential density and AW presence, the AW layer thickness deviates little from the average (Figure 3a and 3b). MKE and EKE are equally important at R2 (Figure 3d). All of these observations support the existence of a continuous southern recirculation pathway at the latitude of R2 that is affected by eddies.

Our results confirm previous findings of westward motion in the central Fram Strait from moorings at this latitude (Beszczynska-Möller et al., 2012; Schauer et al., 2004). Our findings also agree well with observations conducted during the Marginal Ice Zone Experiment with CTD and floats (Bourke et al., 1988; Gascard et al., 1988, 1995; Quadfasel et al., 1987) and later CTD measurements (Gascard et al., 1995; Marnela et al., 2013; Richter et al., 2018; Rudels et al., 2005). They reveal either westward motion, high temperature and salinity, or both between 78°30'N and 79°N. Note, however, that those observations only reveal snapshots, all taken during summer. Observations of recirculation of AW between 78°30'N and 79°N suggest some variability to the whereabouts of the southern recirculation pathway. A longer time series (12 years) of zonal velocities in central Fram Strait from a nearby mooring at 78°50'N reveals only few months during which the flow was not westward (not shown), pointing to broadening/narrowing of the flow north and south of 78°50'N rather than meandering around the location of R2. Further west in the EGC, de Steur et al (2014) found the contribution of the recirculation in long-term measurements to be substantial between 78°50'N and 79°N. If the flow is topographically guided, the Spitsbergen Fracture Zone may act as a one-sided bottleneck, guiding the southern recirculation northwestward until it has passed and reaches the southward flowing EGC.

Model studies also support the existence of a southern recirculation pathway (Hattermann et al., 2016; Kawasaki & Hasumi, 2016; Schlichtholz & Houssais, 1999; Wekerle et al., 2017). These simulations also suggest that the southern recirculation is not necessarily at exactly 78°50'N. In the recent FESOM run summarized in Section 2.4, westward velocities of the southern recirculation are weaker in the model and located further south in the two-year average compared to the observations (Figure 4c). The AW layer is thicker at the latitudes of R1 and R2 in the model (~50–100 m more than in the observations), as well as warmer and more saline (Figure 4a and 4b). EKE and MKE are equally important at the location of the southern recirculation in the model, which compares favorably to our observations (Figure 4d). At R2, where we observe the southern recirculation, EKE plays a larger role in the model.

In summary, we have confirmed the presence of a southern recirculation pathway throughout the year at R2 (78°50'N), however it may broaden/narrow slightly, since it has been observed slightly further north and south in the past. We cannot resolve its precise latitudinal extent, only that the southern recirculation is absent at R1 (78°10'N) and (most of the time) at R3 (79°30'N).

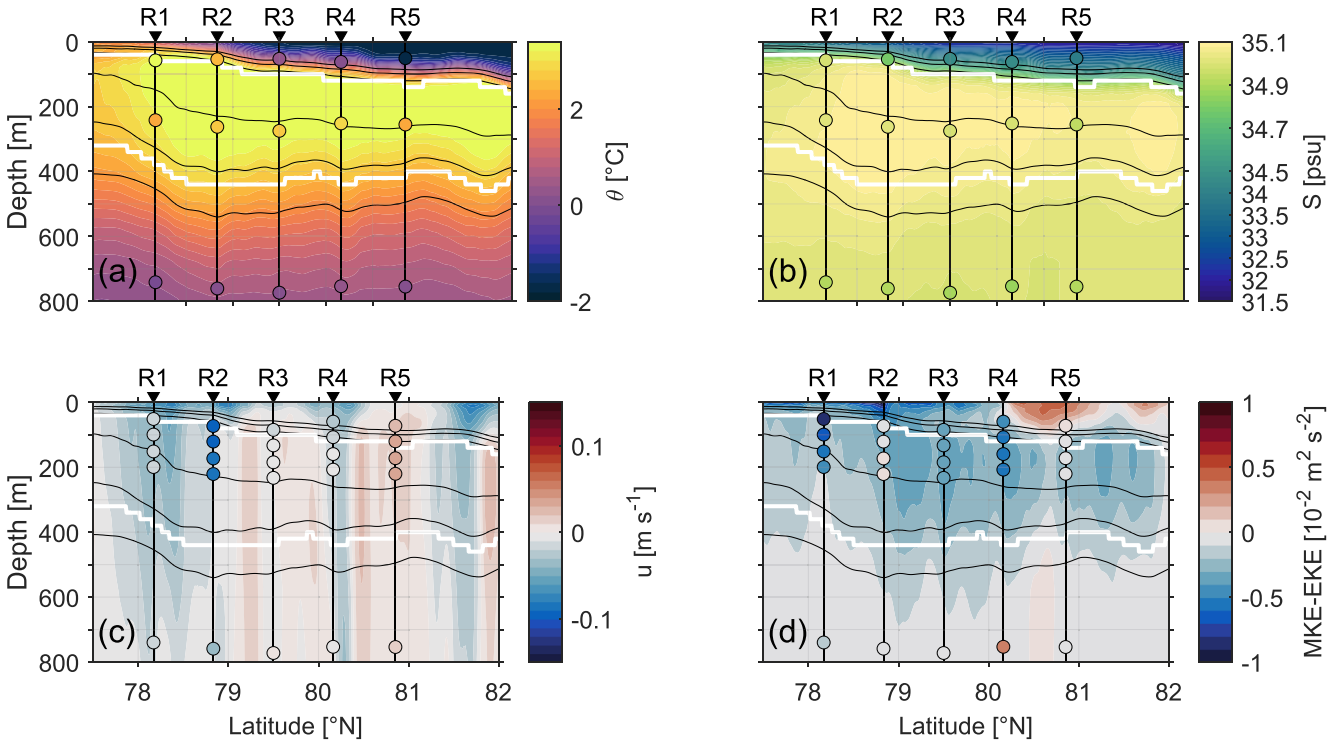

Figure 4. Gridded model sections of (a) potential temperature (°C), (b) salinity (psu), (c) zonal velocity (m s^{-1}), and (d) mean kinetic energy (MKE) minus eddy kinetic energy (EKE) (m^2 s^{-2}), averaged over the observational time series (August 2016–July 2018). Note the nonlinear color bar of salinity. The black lines mark the 27.3, 27.5, 27.7, 27.9, 27.95, and 28 kg m^{-3} isopycnals. The white lines mark the lower and upper boundary of the Atlantic Water (AW) layer in the model. Colored dots show the direct measurements of the instruments installed on the five moorings, averaged over the entire time series.

3.2. Northern Recirculation (R4)

The AW layer thickness at R4 (80°10'N) is generally much smaller than at R2, but similar to that at R3 (79°30'N, Figure 2). Nonetheless, its value deviates from the mean quite strongly, at peak times being almost as large as at R2 (Figure 3). Potential temperature strongly varies at R4, as increased thickness of the AW layer toward the surface at times eliminates the cold, fresh surface layer (Figure 3a). Salinity varies most with the varying sea ice cover, as can be seen close to the surface at R3 and R4 in Figure 3b. The EKE has a subsurface maximum at R4 at 200 m depth (Figure 3c), i.e., near the upper boundary of the AW layer. On average, velocities at R4 are southward (Figure 2d), suggesting that R4 is located in the Arctic Ocean outflow region. However, southward velocities are smallest in the AW layer, at the same depth as the EKE maximum. We observe no westward velocities in the two-year average (Figure 2d). The difference between MKE and EKE reveals EKE to dominate at R4, with the MKE of the Arctic Ocean outflow only dominating at greater depths at R4 (Figure 3d). All of these observations support the existence of a highly variable northern recirculation pathway that transports eddies to the prime meridian at the latitude of R4, which are then carried southward with the Arctic Ocean outflow.

Our observations of the northern recirculation pathway agree well with observations conducted during the Marginal Ice Zone Experiment with CTD and floats (Bourke et al., 1988; Gascard et al., 1988, 1995; Quadfasel et al., 1987) and later CTD measurements (Richter et al., 2018), which also find a northern recirculation pathway at ~80°N. The northern recirculation pathway was often observed further east than our measurements (likely due to the ice cover impeding measurements at 0°EW), where it displayed both a temperature and salinity maximum, as well as westward velocities. Model studies support the existence of a northern recirculation pathway (Hattermann et al., 2016; Kawasaki & Hasumi, 2016; Schlichtholz & Houssais, 1999). Further east than our observations at 2°45'E, Wekerle et al. (2017) found high westward AW transport at 80°N during winter, although the transport was much weaker during summer. The location of R4 in their

model was in the Arctic Ocean outflow, which agrees with our observations of average southward flow at R4.

In the recent FESOM run summarized in Section 2.4, averaged over the observational period of August 2016 to July 2018, we find weak westward velocities and high potential temperature and salinity at the latitude of R4 (Figure 4). The AW layer thickness in the model decreases very little toward the north and, based on the presence of AW, the model suggests that the northern rim of the recirculation is only reached at 83°30'N (not shown). We observe decreasing AW layer thickness toward the north at the moorings, and already very little AW at R5 (80°50'N). There appears to be another recirculation pathway at 81°50'N in the model, with westward motion as well as a maximum in potential temperature and salinity (Figure 4). EKE dominates the AW layer, whereas MKE is larger than EKE only in the surface Arctic Ocean outflow between R4 and R5. Overall, the performance of the model appears to be poorer for the northern recirculation than the southern recirculation. In the north, the recirculating AW is confronted with colder, fresher surface waters and sea ice cover, and ultimately has to subduct below this surface layer. This process happens on not only the mesoscale, but also the submesoscale (von Appen et al., 2018) and is not yet fully understood. The horizontal resolution of the model as well as of the forcing applied is not sufficient to resolve the submesoscale. Additionally, the dynamics of the upper water column might not be well represented with a 10 m vertical resolution.

In summary, we find that the northern recirculation is present at R4 (80°10'N) as passing eddies that introduce high variability to velocity observations and the amount of AW that is available to be transported southward with the Arctic Ocean outflow. It is possible that the northern recirculation exists as a mean flow further east.

4. Variability of the Atlantic Water Recirculation

4.1. Seasonal Variability

Of all the variables indicative of AW recirculation, monthly means of salinity vary little for the southern recirculation at R2 (Figure 5b) and flow direction is mostly westward throughout the time series (Figure 5f and 5g). We observe a seasonal cycle in potential temperature, AW layer thickness, EKE, flow strength and direction at R2. Potential temperature is minimal in spring (Figure 5a). EKE is maximal in spring, after which both potential temperature and AW layer thickness increase (Figure 5a and 5c). This agrees with observations by von Appen et al. (2016), who found EKE in central Fram Strait at the latitude of R2 to be maximal in March/April, lagging the maximum in the WSC at the same latitude by 1–2 months. This indicates a larger role of eddies from the WSC for the southern recirculation during spring. During spring, we also observe the flow direction to be northwestward and stronger in magnitude than during the rest of the year (Figure 5f and 5g). However, we do not observe this seasonal cycle in flow direction and strength from a longer time series of a nearby mooring, so it is not a robust signal.

The seasonal cycle of potential temperature and AW layer thickness is more pronounced during the first year (2016/17), when the location of R2 was partially covered by ice (Figures 5e and 6a). Under these circumstances, the seasonal cycle of the parameters indicative of AW recirculation is likely affected both by the seasonality of the recirculation itself as well as that of the ice cover (e.g., the maximum potential temperature is only reached after the ice is gone in August, Figure 5a and 5e). During the second year the ice is absent at R2 (Figures 5e and 6b) and, in addition to the seasonal cycle of the recirculation, heat and momentum exchange between atmosphere and ocean likely play a larger role throughout the year. We conclude that the southern recirculation is a phenomenon that never fully disappears, but is affected by eddies from the WSC more strongly in spring. Since the AW is so close to the surface at R2, it is likely in contact with the atmosphere when there is no ice.

From our observations it is not fully clear whether the southern recirculation is related to a current advecting eddies from the WSC or to self-propagating eddies. On average, we find EKE and MKE to be equally important (Figure 3d). During spring, EKE dominates, while during most other months, MKE dominates (not shown). This suggests a mean flow branching off the WSC, as well as eddies passing the mooring R2. The eddies could be shed by the WSC and either be advected by the mean flow, or topographically guid-

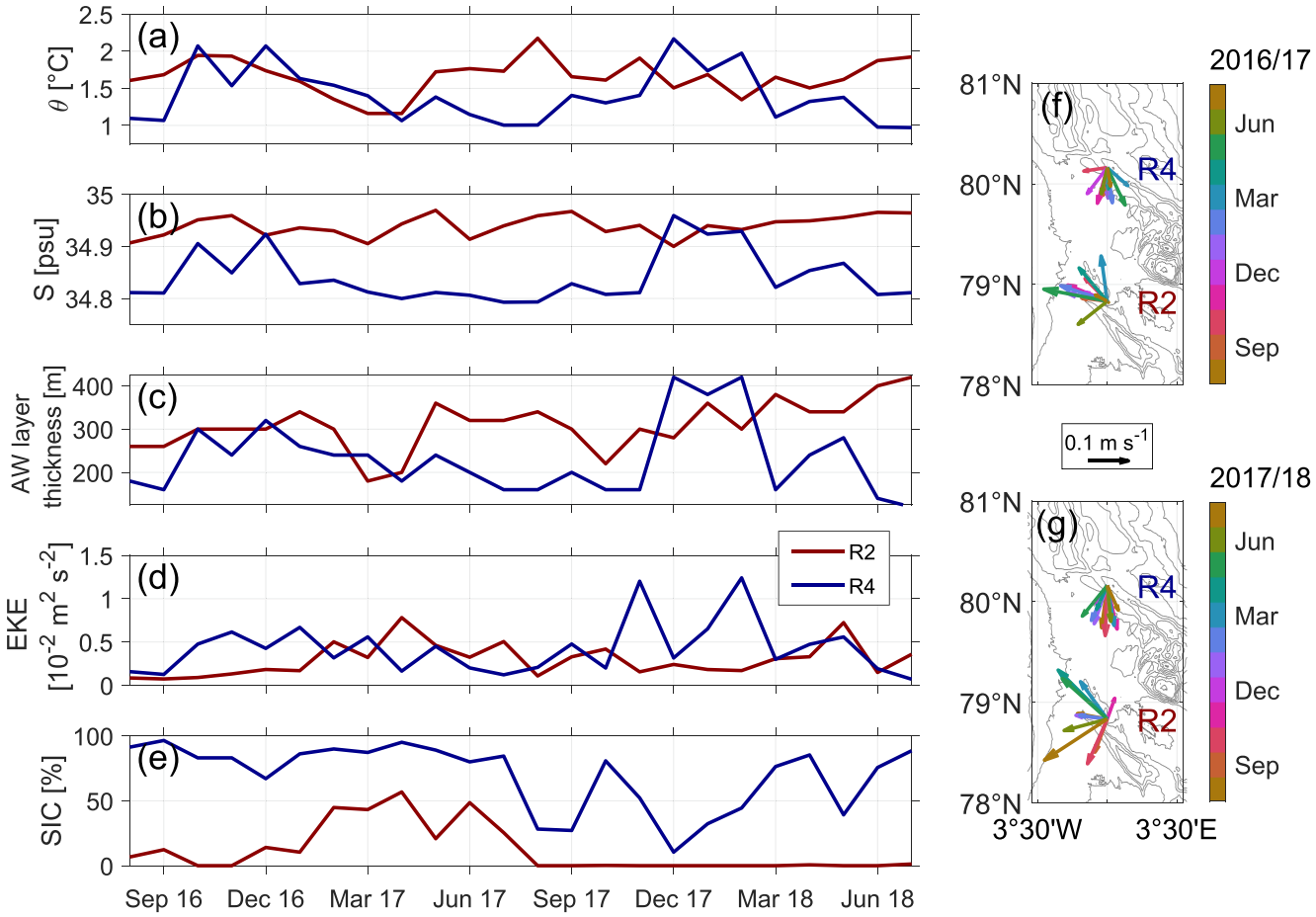

Figure 5. Monthly means at moorings R2 (red), and R4 (blue) of column averaged (20/40–800 m) (a) potential temperature (°C), (b) salinity (psu), (c) AW layer thickness (m), (d) eddy kinetic energy (EKE) (10^{-2} m^2 s^{-2}), and (e) sea ice concentration (SIC) (%) from satellite data. Column averaged (20–800 m) flow direction and strength at the three mooring locations for each month of (f) the first year (2016/17) and (g) the second year (2017/18) of observations, with bathymetry from Schaffer et al. (2019).

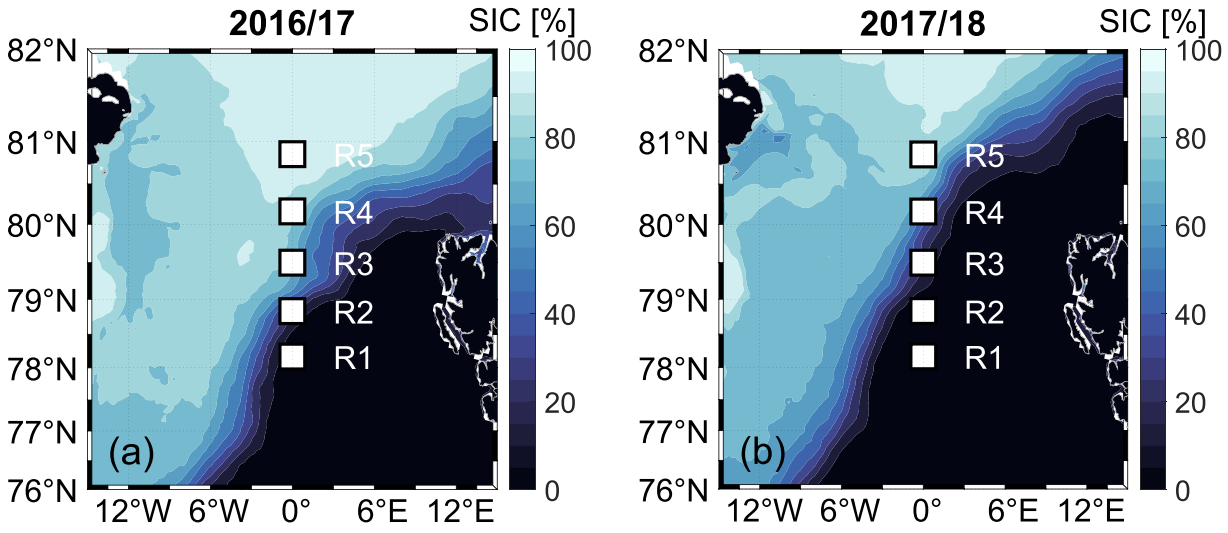

Figure 6. Maps of sea ice concentration (SIC) (%) in Fram Strait averaged over (a) the first (August 2016–July 2017), and (b) the second year of observations (August 2017–July 2018). Mooring locations are marked as white squares.

ed along the Spitsbergen Fracture Zone. The seasonal cycle of EKE and baroclinic instability observed by von Appen et al. (2016) suggests so. It also seems feasible that the recirculation branch itself is subject to baroclinic instability and the generation of eddies, though this may be a process accounting for less of the total variability. The instability in central Fram Strait presumably is due to the large horizontal density gradients between AW and Polar Water there. Baroclinic instability slumps these horizontal density gradients to vertical density gradients, which may mediate the subduction of AW below Polar Water (Hattermann et al., 2016). Consistently, in two eddy resolving models, Wekerle et al. (2020) found the main generation region of eddies that follow the southern recirculation pathway to be the central Fram Strait and not the WSC. However, they find barotropic and baroclinic instability to be much more efficient (accounting for larger mean to eddy energy transfers) in the WSC than in central Fram Strait.

All variables indicative of AW recirculation display a strong seasonal cycle for the northern recirculation at R4, with the exception of flow strength and direction, which is weak and southward throughout both years (Figure 5f and 5g). Potential temperature, salinity, and AW layer thickness all peak in late autumn/winter, specifically in October–December 2016 and December 2017 to February 2018, and are minimal during summer (Figure 5a–5c). Compared to the atmospheric forcing, these variations are delayed by a few months and thus very likely an advected signal. EKE is maximal in both years during late autumn/winter, with the maxima in the second year (November 2017 and February 2018) substantially exceeding the ones in the first year (October/November 2016 and January 2017) (Figure 5d). The large variability between the monthly means of EKE during the second winter suggests processes on shorter timescales than months to be important that are masked by this averaging. During the second year, the sea ice cover is more variable than during the first year (Figure 5e), this potentially being a contributing factor to the variability of EKE.

The stronger EKE maximum and the higher AW layer thickness during winter 2017/18 suggest more AW recirculation. At 78°50'N the front between AW and the colder, fresher water of the western Fram Strait was located further east in 2002–mid-2015 than in mid-2015–2018, with the exception of winter 2016/17, which was more representative of the earlier period (Laura de Steur, pers. comm., 2020). The implication for our observation is that the second winter (2017/18) is much more representative of the recent situation in Fram Strait, with more AW recirculating north of the Molloy Hole and being transported southwards with the EGC. We can conclude that the northern recirculation at 0°EW is a seasonal phenomenon that is absent during summer, but present and highly variable at the mesoscale during winter. The frontal position in the previous years implies that the northern recirculation has become stronger in recent years.

Unlike the southern recirculation, we do not observe the northern recirculation as a westward flow of AW, but rather as periods of increased AW layer thickness and EKE. Further east than 0°EW it was, however, observed and modeled as westward flow of AW (e.g., Gascard et al., 1988; Wekerle et al., 2017). It is possible that this flow circulates around the Molloy Hole and may even join the southern recirculation. In the past, a cyclonic gyre or large eddy was observed close to the Molloy Hole (Bourke et al., 1987; Quadfasel et al., 1987). Similar to the southern recirculation we can only speculate whether the AW eddies we observe at 0°EW are generated by the WSC and advected by the mean flow or topographically steered, or generated by recirculating flow outside the WSC. The proximity to the WSC of R4 (compared to R2) makes at least some eddies originating from the WSC seem likely and, in two models, Wekerle et al. (2020) found that most eddies following the path of the northern recirculation originated in the WSC, specifically anticyclones. If the northern recirculation exists as a mean flow that circulates around the Molloy Hole, a pertinent question is how eddies are able to detach from this mean flow and join the EGC at R4. A factor we have not yet considered is the proximity of the marginal ice zone at R4. Besides the commonly accepted eddy generation mechanisms of barotropic/baroclinic instability–mean flow interacting with a seamount–and topographic steering due to conservation of potential vorticity, Johannessen et al. (1987) proposed the generation of ice edge eddies. This is related to the subduction of AW below colder, fresher surface water associated with sea ice, which affects the water mass' vorticity—a process clearly related to mesoscale variability that is not yet well understood. Furthermore, wind-induced differential Ekman pumping along a meandering ice edge may generate upper ocean eddies (Johannessen et al., 1987).

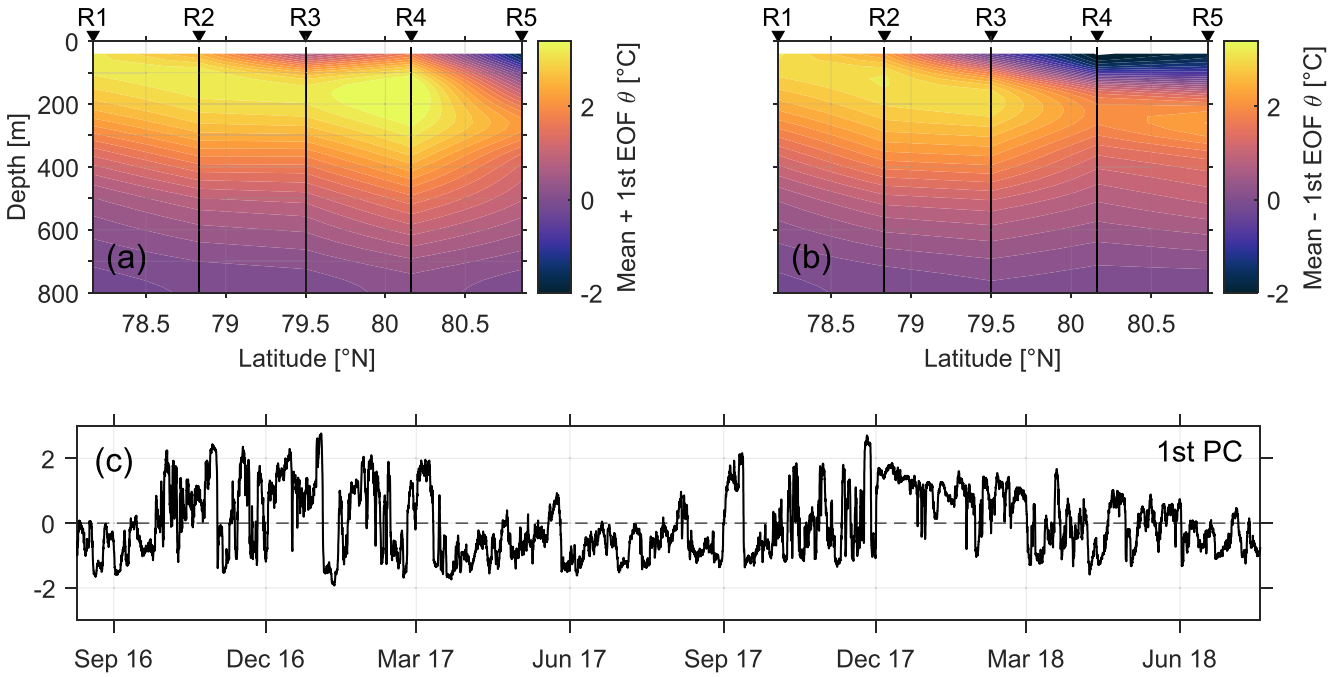

Figure 7. Gridded potential temperature (°C) section, of (a) the mean (see Figure 2a) plus the first empirical orthogonal function (EOF) of potential temperature, and (b) the mean minus the first EOF of potential temperature. The first/second EOF explain 27.17%/13.84% of the variance. (c) Hourly time series of the first principal component (PC) of potential temperature.

4.2. Mesoscale Variability

The first empirical orthogonal function (EOF) of the gridded potential temperature of all five moorings and all 40 depth levels reveals that the water mass distribution changes frequently between a prominent AW layer at R4 with almost no colder water above (Figure 7a), and a thin AW layer with a thicker layer of colder water on top (Figure 7b). The other mooring locations contribute much less to this first EOF. The first principal component (PC) displays higher variability in winter, particularly during the first one (Figure 7c). This variability clearly happens on shorter timescales than seasonal, and is likely associated with mesoscale eddies, as already suggested by the high EKE, or even submesoscale features and waves. During summer 2017, a time during which there was prolonged high sea ice concentration at R4 (Figure 5e), a situation was established where there was cold water on top of the AW (Figure 7b). When there was prolonged low sea ice concentration, which was only the case in winter 2017/18 (Figure 5e), the situation established is the one with a thick AW layer reaching almost to the surface (Figure 7a). The first PC of potential temperature and the time series of AW layer thickness at R4 are significantly correlated with a correlation coefficient of 0.87.

In order to further evaluate the situations described by the first EOF of potential temperature, we attempt to identify events of strong recirculation at mooring R4 associated with eddy activity. We use EKE as an indicator and find seven events that exceed a daily average of 0.015 $m^2 s^{-2}$ during the first year (2016/17), and eight events that exceed the same threshold during the second year (2017/18). The most extreme example of such an event, which occurred between November 19 and December 3, 2017, shows the average southward flow at R4 being disturbed by strong northwestward velocities that then change to southeastward velocities within a day (Figure 8c and 8d). This change is accompanied by water with high potential temperature and salinity, fitting the AW definition and reaching from close to the surface down to 800 m (Figure 8a and 8b). It results in a depression of the middepth isopycnals by more than 300 m. This is a prime example of a mesoscale anticyclonic eddy carrying AW, which passes the location of R4 within about a week. The mean properties of anticyclones originating from the WSC that commonly pass this location in the two models analyzed by Wekerle et al. (2020) generally compare well with our example. Figure 8 shows the strongest event that we observe, with deeper and stronger maxima of potential temperature and salinity than the mean properties of Wekerle et al. (2020), but a similar vertical structure.

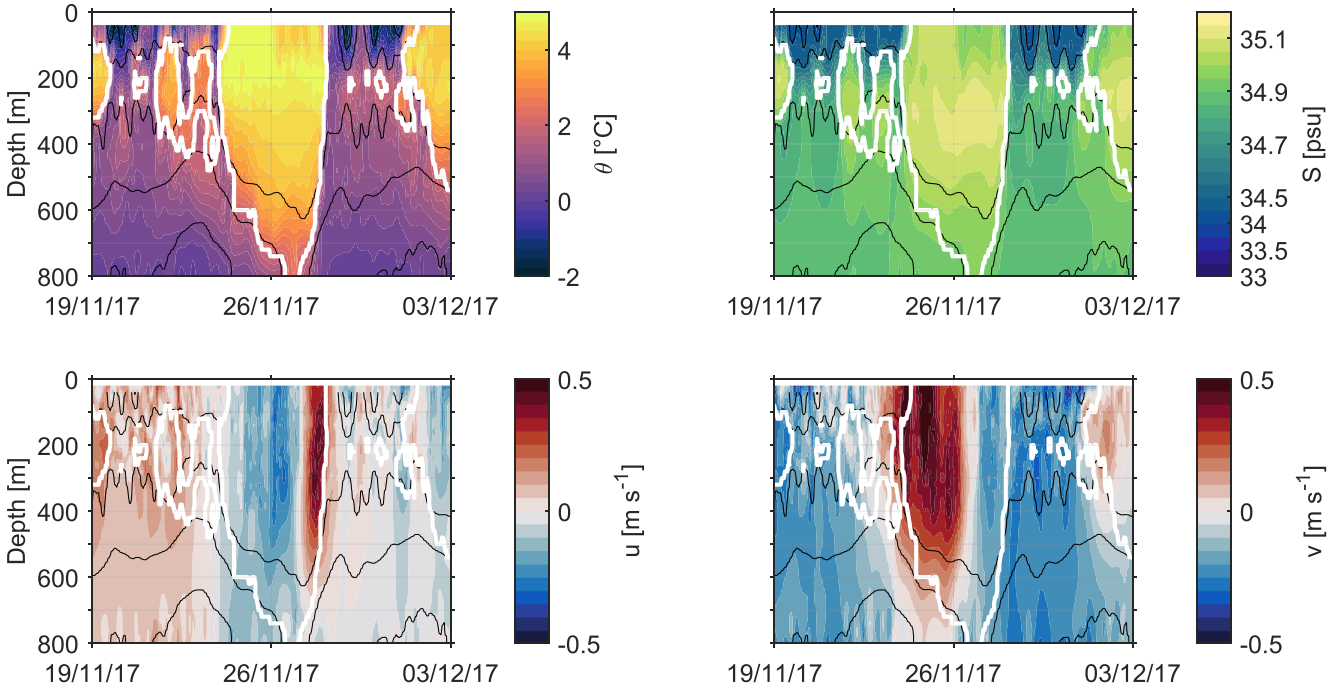

Figure 8. Hovmöller diagrams of gridded (a) potential temperature (°C), (b) salinity (psu), (c) zonal velocity (m s^{-1}), and (d) meridional velocity (m s^{-1}) at R4 from November 19 to December 3, 2017. Note the nonlinear color bar of salinity. The black lines mark the 27.5, 27.7, 27.9, 27.95, and 28 kg m^{-3} isopycnals. The white lines mark the boundaries of the AW layer.

All of these events were associated with a strong increase and subsequent decrease in AW layer thickness, usually happening on the timescale of a couple of days up to two weeks (Figure 9b). There are no events in summer. Events occurred during late autumn/early winter, when the sea ice concentration was low or highly variable (blue events, Figure 9c). They also occurred during late winter/early spring, when the sea ice concentration was high (red events, Figure 9c). Notably there is only one occasion when there is sustained above–average AW layer thickness over 1–2 months (Figure 9b), which is during December 2017/January 2018, when there is almost no sea ice cover (Figure 9c). This is preceded by the strongest event in the time series (Figure 8). An interesting question is whether the recirculation of AW and sea ice affect each other. Different forms of interaction are possible. We will discuss, below, potential interactions. While we cannot conclude their relative importance or validity from our analysis, they may stimulate further discussion.

The recirculation may affect the sea ice by providing heat to melt it. Indeed, at times we observe AW up to at least 40 m depth (i.e., our uppermost measurements). The AW recirculation constitutes a westward transport of heat in Fram Strait, from the AW at the surface in the east toward the sea ice at the surface in the west. Some of this heat likely contributes to sea ice melt before the AW subducts below the sea ice. In the cases when we observe high AW layer thickness and high sea ice concentration at R4, the AW has already subducted below the colder, fresher surface waters associated with sea ice presence. Both the recirculation and the sea ice cover may be governed by wind, as the latter largely depends on the export of ice from the Arctic Ocean (Kwok et al., 2004; Ricker et al., 2018). We have not touched upon the subject of the wind being a driver of the recirculation in Fram Strait in this study, but one should consider that it may be a factor as well and adds another level of complexity to this interaction.

Sea ice in Fram Strait is advected into the region, e.g., from the Laptev Sea (Krumpen et al., 2019), rather than being formed locally through freezing. Sea ice provides meltwater, which increases upper ocean stratification. As a result, higher sea ice concentration in central Fram Strait can be considered a proxy for stronger upper ocean stratification. Consequently, the presence of sea ice may change the stratification, creating strong density gradients that in turn may affect the recirculation by forcing the AW to subduct deeper below the PW. The core of the WSC is generally weakly stratified during winter (von Appen et al., 2016) and thus a region of low potential vorticity. In summer it is temperature stratified, which means its potential vorticity

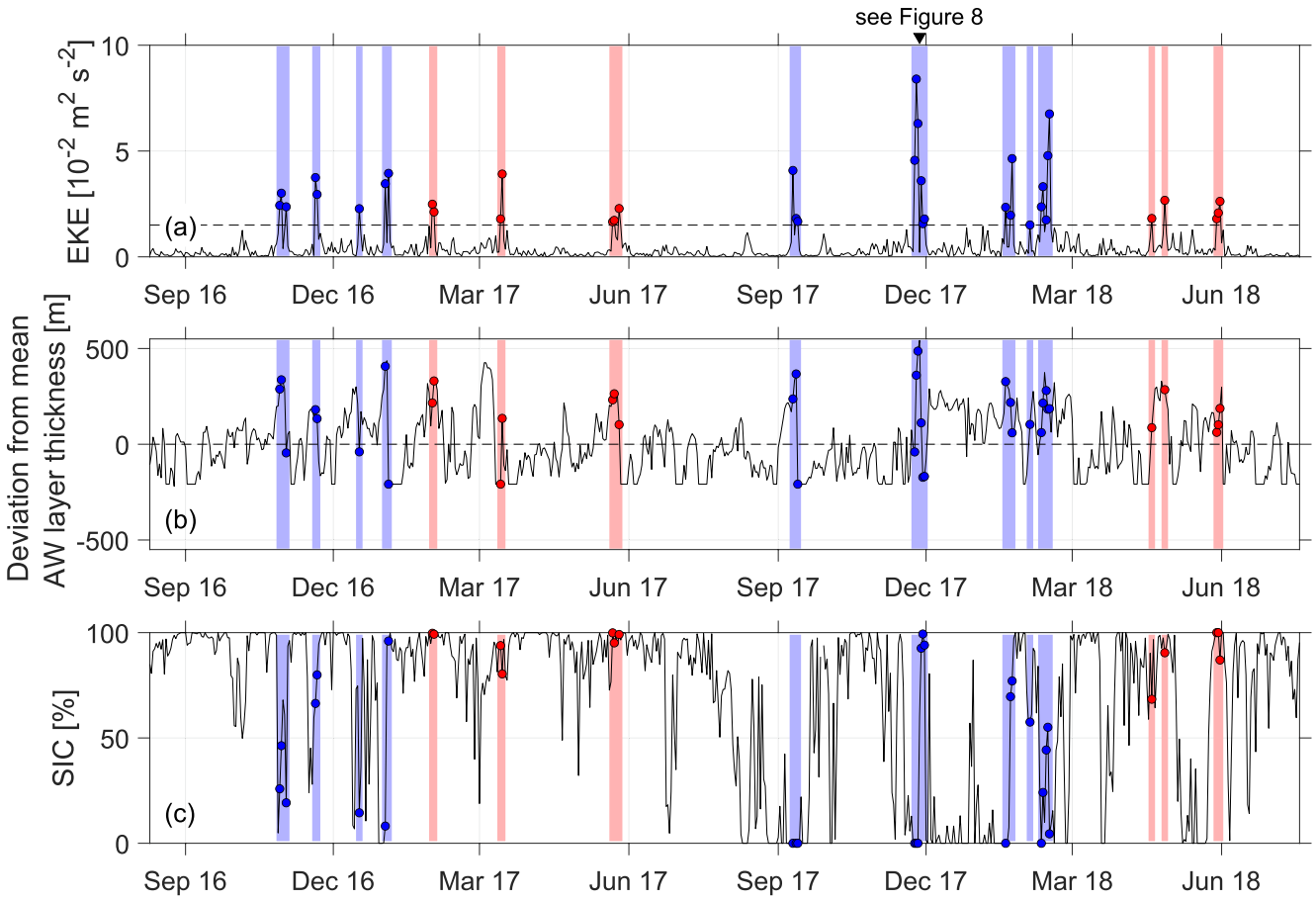

Figure 9. Daily time series of (a) eddy kinetic energy (EKE) ($m^2\ s^{-2}$), (b) deviation from mean Atlantic Water (AW) layer thickness (m), which is 208 m averaged over the entire time series, and (c) sea ice concentration (SIC) (%) at R4. Times, during which EKE exceeded 0.015 $m^2\ s^{-2}$, as indicated by the dotted line in panel (a), are highlighted with colored shading, as well as circles for the individual values. We differentiate between the occurrence of these EKE peaks during low/variable SIC (blue) and high SIC (red) at R4. The event shown in Figure 8 is highlighted.

is higher than in winter but smaller than in the strongly salinity stratified central Fram Strait. There the absence of sea ice (and thus meltwater) will correspond to strong stratification and high potential vorticity, while ice presence will result in very strong stratification/very high potential vorticity. During times when there was high sea ice concentration in central Fram Strait, it was highly stratified and thus a region of high potential vorticity. A water parcel that is transported from the WSC to the central Fram Strait (i.e., that recirculates), must conserve its potential vorticity ($PV = (f + \zeta)/H$, where f is the Coriolis parameter, ζ is the relative vorticity, and H is the vertical extension of the water parcel), assuming that frictional effects and turbulence are small. When it is subducted below the PW, its H changes and, to conserve potential vorticity, so must its ζ. We presume that H needs to change more, if the AW has to subduct deeper, i.e., when the stratification in central Fram Strait is stronger. Depending on whether the eddy is a cyclone or an anticyclone, this process weakens or strengthens the eddy and therefore furthers or limits recirculation of AW. The interaction between the recirculation and the ice edge may even generate new eddies.

Johannessen et al. (1987) first proposed the generation of ice edge eddies. Gascard et al. (1988) further described these ice edge eddies as the result of the interaction between open ocean eddies and the EGC and considered them to be the most important eddy generation mechanism in central Fram Strait. Eddies may still be shed by the WSC and travel westwards in central Fram Strait, but are modified or even newly generated, once they meet the sea ice and the colder, fresher waters of the western Fram Strait. Gascard et al. (1988) found these ice edge eddies to not change in size, but in speed, becoming up to two times faster due to the interaction with the ice edge. One interpretation is that the events of high EKE that we

observe in late autumn/early winter (Figure 9a, in blue) may also be weak WSC eddies that are enhanced by the interaction with the nearby ice edge (as indicated by the variable ice cover at R4, Figure 9c). Events in late winter/early spring (Figure 9a, in red) would then represent eddies that have already gone through the process of subduction. This does not, however, explain why these events are weaker, as the EKE signal from the WSC should be stronger during this time of the year. At this point it remains unclear, whether the interaction with the sea ice edge is conducive of recirculation or not, but an interaction certainly takes place.

The recirculation may affect the sea ice, as well as that the sea ice may affect the recirculation. We have discussed different interactions. While each of these processes may explain the eddy activity, we cannot determine the relative importance of these interactions from our data set.

5. Conclusions

Our aim was to narrow down the location of the AW recirculation, present direct observations of its seasonality, and gather a better understanding of its mesoscale variability. We have confirmed the presence of two recirculation pathways at 78°50'N and 80°10'N on the prime meridian in central Fram Strait, but we cannot determine their precise meridional extent. They are characterized by different properties, seasonal and mesoscale variability.

The southern recirculation has previously been observed and modeled between 78°30'N and 79°N. While it may be subject to some broadening and narrowing, our observations clearly indicate that it is present at 78°50'N throughout the year. In addition, we do not observe any recirculation at 78°10'N and little recirculation at 79°30'N, further delimiting the location of this recirculation pathway. We observe it as a mean flow, which is affected by eddies, with the latter having the largest effect in spring. This agrees well with observations by von Appen et al. (2016) of the seasonal cycle of instabilities in the WSC and EKE along 78°50'N. These observations suggest that the eddies either originate in the WSC and are advected by the mean flow of the recirculation branch, or that they originate in the recirculation branch itself, provided it is subject to similar instabilities. We may also observe self-propagating eddies with a westward propagation speed, as suggested by previous studies (Bashmachnikov et al., 2020; Wekerle et al., 2020).

The northern recirculation, in contrast, is observed solely as passing eddies at 80°10'N on the prime meridian. It has previously been observed and modeled as a westward flow further east, which likely circulates around the Molloy Hole and does not reach as far west as 0°EW. We observe a strong seasonality of the northern recirculation, with it being strongest in late autumn and winter, and absent during summer. This seasonality had previously been suggested by model studies (Hattermann et al., 2016; Wekerle et al., 2017), but no observational data had been available thus far. The passing eddies of the northern recirculation result in frequent changes between a thick AW layer that may reach up to the surface and a thin AW layer with colder, fresher water on top. These eddies likely originate from the WSC and are either advected by the mean recirculation flow further east or self-propagate westwards. The interaction with the sea ice edge, where AW meets colder, fresher surface waters and ultimately has to subduct below the ice, plays a much larger role for the northern recirculation than the southern one. We speculate that this interaction may weaken or strengthen pre-existing open ocean eddies, or even create new ones.

We compared our findings to an eddy-resolving ocean-sea ice model. While it captured the properties of the southern recirculation well, its performance was poorer on the northern recirculation, where mesoscale and likely submesoscale variability played a much larger role. The model over-estimated the thickness of the AW layer and its presence in the north, with the northern rim of the recirculation at 83°30'N, while we observed very little AW 300 km further south at 80°50'N. This means that (sub-)mesoscale processes along the ice edge, as well as the drivers that partition the WSC into Arctic Ocean inflow and recirculation, might benefit from future model improvements as they are dynamically very important for the recirculation. If these aspects were modeled better, it should be possible to calculate transports more robustly in the future.

At high latitudes, currents are thought to be much more guided by bottom topography than at low latitudes (Trodahl & Isachsen, 2018). That is, they more commonly follow f/H contours (where H is the water depth) to conserve potential vorticity. If this also applies to the recirculation with its branches along the Spitsber-

gen Fracture Zone and the Molloy Fracture Zone, then this may mean that its interannual variability is fairly weak. This contrasts with a scenario where it might be driven more by atmospheric forcing with its inherent large interannual variability.

The moorings were originally placed with the goal of observing the recirculation's location and variability, as we have discussed in this study. The distance between the moorings as well as the fact that we observe the northern recirculation solely as passing eddies makes it impossible for us to quantify transports. Changing the locations of some of the moorings for possible future deployments could be helpful in this regard and help answer remaining open questions. Here we suggest a possible future mooring array design. If moorings were installed at the southern (78°30'N) and northern rim (79°N) of previous accounts of the southern recirculation, it should be possible to further delimit its location at the prime meridian. While we do not include further analysis of data from R3 (79°30'N) in this study, a longer time series from this location might give insights to the variability of the recirculation. It may be affected by the southern recirculation at times, and receives a signal from the northern recirculation via the Arctic Ocean outflow. Hence, a mooring should be placed at 79°30'N in the future. The high variability at R4 (80°10'N) and its proximity to the ice edge makes it the most valuable for studying eddies and thus observations at this location should be continued. Another mooring could be positioned further east, north of the Molloy Hole, with the goal of capturing a more continuous flow of the northern recirculation and gathering a better understanding of its relationship with the WSC under more ice-free conditions.

Using the first year-round observations, this study was able to improve our knowledge of the recirculation's location and variability. These are necessary for future work on transport estimates and the control mechanisms of the recirculation, the latter including the generation and propagation of eddies in Fram Strait, as well as the subduction of AW below the fresher, colder waters of the western Fram Strait.

Data Availability Statement

Observational data are available at https://doi.org/10.1594/PANGAEA.904565 (R moorings), https://doi.org/10.1594/PANGAEA.900883 (other moorings), https://doi.org/10.1594/PANGAEA.898400 (AMSR2 sea ice concentration), https://doi.org/10.1594/PANGAEA.919778 (AMSR-E sea ice concentration). Model data are available at http://doi.org/10.5281/zenodo.4696124.

Acknowledgments
Support for this study was provided by the Helmholtz Infrastructure Initiative FRAM (FRontiers in Arctic marine Monitoring). Ship time was provided under Grant No. AWI_PS100_01 and AWI_PS114_01. For both cruises, the efforts of captain and crew of RV Polarstern are greatly appreciated. The authors gratefully acknowledge the funding by the Deutsche Forschungsgemeinschaft (DFG, German Research Foundation) - Projektnummer 268020496 - TRR 172, within the Transregional Collaborative Research Center "ArctiC Amplification: Climate Relevant Atmospheric and SurfaCe Processes, and Feedback Mechanisms (AC)^3." The authors thank the editor and the two reviewers for their constructive comments that have helped clarify a number of aspects in the study. Open access funding enabled and organized by Projekt DEAL.

References

Aksenov, Y., Bacon, S., Coward, A. C., & Holliday, N. P. (2010). Polar outflow from the Arctic Ocean: A high resolution model study. *Journal of Marine Systems*, *83*, 14–37. https://doi.org/10.1016/j.jmarsys.2010.06.007

Bamber, J. L., Tedstone, A. J., King, M. D., Howat, I. M., Enderlin, E. M., van den Broeke, M. R., & Noel, B. (2018). Land ice freshwater budget of the arctic and north Atlantic oceans: 1. Data, methods, and results. *Journal of Geophysical Research: Oceans*, *123*, 1827–1837. https://doi.org/10.1002/2017JC013605

Bashmachnikov, I. L., Kozlov, I. E., Petrenko, L. A., Glok, N. I., & Wekerle, C. (2020). Eddies in the North Greenland Sea and Fram Strait from Satellite Altimetry, SAR and High-Resolution Model Data. *Journal of Geophysical Research: Oceans*, *125*, e2019JC015832. https://doi.org/10.1029/2019JC015832

Beszczynska-Möller, A., Fahrbach, E., Schauer, U., & Hansen, E. (2012). Variability in Atlantic water temperature and transport at the entrance to the Arctic Ocean, 1997–2010. *ICES Journal of Marine Science*, *69*(5), 852–863. https://doi.org/10.1038/278097a0

Bourke, R. H., Tunnicliffe, M. D., Newton, J. L., Paquette, R. G., & Manley, T. O. (1987). Eddy near the Molloy Deep Revisited. *Journal of Geophysical Research*, *92*(C7), 6773–6776. https://doi.org/10.1029/JC092iC07p06773

Bourke, R. H., Weigel, A. M., & Paquette, R. G. (1988). The westward turning branch of the West Spitsbergen current. *Journal of Geophysical Research*, *93*(C11), 14065–14077. https://doi.org/10.1029/jc093ic11p14065

Crews, L., Sundfjord, A., & Hattermann, T. (2019). How the Yermak pass branch regulates Atlantic water inflow to the Arctic Ocean. *Journal of Geophysical Research: Oceans*, *124*, 267–280. https://doi.org/10.1029/2018JC014476

de Steur, L., Hansen, E., Mauritzen, C., Beszczynska-Möller, A., & Fahrbach, E. (2014). Impact of recirculation on the East Greenland Current in Fram Strait: Results from moored current meter measurements between 1997 and 2009. *Deep-Sea Research Part I*, *92*, 26–40. https://doi.org/10.1016/j.dsr.2014.05.018

Dee, D. P., Uppala, S. M., Simmons, A. J., Berrisford, P., Poli, P., Kobayashi, S., et al. (2011). The ERA-Interim reanalysis: Configuration and performance of the data assimilation system. *Quarterly Journal of the Royal Meteorological Society*, *137*, 553–597. https://doi.org/10.1002/qj.828

Fieg, K., Gerdes, R., Fahrbach, E., Beszczynska-Möller, A., & Schauer, U. (2010). Simulation of oceanic volume transports through Fram Strait 1995-2005. *Ocean Dynamics*, *60*, 491–502. https://doi.org/10.1007/s10236-010-0263-9

Gascard, J.-C., Kergomard, C., Jeannin, P.-F., & Fily, M. (1988). Diagnostic study of the Fram Strait marginal ice zone during summer from 1983 and 1984 Marginal ice zone experiment Lagrangian observations. *Journal of Geophysical Research*, *93*(C4), 3613–3641. https://doi.org/10.1029/jc093ic04p03613

Gascard, J.-C., Richez, C., & Rouault, C. (1995). New insights on large-scale oceanography in Fram Strait: The West Spitsbergen Current. In W. O. Smith, Jr, & J. M. Grebmeir (Eds.), *Coastal and estuarine studies*, (pp. 131–182). American Geophysical Union. https://doi.org/10.1029/CE049p0131

Hansen, B., & Østerhus, S. (2000). North Atlantic – Nordic Seas exchanges. *Progress in Oceanography*, *45*, 109–208. https://doi.org/10.1111/j.1751-8369.2001.tb00053.x

Hattermann, T., Isachsen, P. E., von Appen, W.-J., Albretsen, J., & Sundfjord, A. (2016). Eddy-driven recirculation of Atlantic Water in Fram Strait. *Geophysical Research Letters*, *43*, 3406–3414. https://doi.org/10.1002/2016GL068323

Håvik, L., Pickart, R. S., Våge, K., Torres, D. J., Thurnherr, A. M., Beszczynska-Möller, A., et al. 2017). Evolution of the East Greenland Current from Fram Strait to Denmark Strait: Synoptic measurements from summer 2012. *Journal of Geophysical Research: Oceans*, *122*, 1974–1994. https://doi.org/10.1002/2017JC012961

Hofmann, Z. (2020). *Seasonal variability of Atlantic Water recirculation in Fram Strait from observations (Master thesis, Christian-Albrechts-Universität zu Kiel)*. Retrieved from https://epic.awi.de/id/eprint/52224/

Ilicak, M., Drange, H., Wang, Q., Gerdes, R., Aksenov, Y., Bailey, D., et al. (2016). An assessment of the Arctic Ocean in a suite of interannual CORE-II simulations. Part III: Hydrography and fluxes. *Ocean Modelling*, *100*, 141–161. https://doi.org/10.1016/j.ocemod.2016.02.004

Johannessen, J. A., Johannessen, O. M., Svendsen, E., Shuchman, R., Manley, T. O., Campbell, W. J., et al. (1987). Mesoscale Eddies in the Fram Strait Marginal Ice Zone during the 1983 and 1984 marginal ice zone experiments. *Journal of Geophysical Research*, *92*(C7), 6754–6772. https://doi.org/10.1029/JC092iC07p06754

Kanzow, T. (2017). *The Expeditions PS100 of the Research Vessel POLARSTERN to the Fram Strait in 2016*. Reports on Polar and Marine Research. https://doi.org/10.2312/BzPM_0702_2016

Kawasaki, T., & Hasumi, H. (2016). The inflow of Atlantic water at the Fram Strait and its interannual variability. *Journal of Geophysical Research: Oceans*, *121*, 502–519. https://doi.org/10.1002/2015jc011375

Krumpen, T., Belter, H. J., Boetius, A., Damm, E., Haas, C., Hendricks, S., et al. (2019). Arctic warming interrupts the Transpolar Drift and affects long-range transport of sea ice and ice-rafted matter. *Scientific Reports*, *9*(5459). https://doi.org/10.1038/s41598-019-41456-y

Kwok, R., Cunningham, G. F., & Pang, S. S. (2004). Fram Strait sea ice outflow. *Journal of Geophysical Research*, *109*, C01009. https://doi.org/10.1029/2003jc001785

Manley, T. O. (1995). Branching of Atlantic water within the Greenland-Spitsbergen Passage: An estimate of recirculation. *Journal of Geophysical Research*, *100*(C10), 20627–20634. https://doi.org/10.1029/95JC01251

Marnela, M., Rudels, B., Houssais, M.-N., Beszczynska-Möller, A., & Eriksson, P. B. (2013). Recirculation in the Fram Strait and transports of water in and north of the Fram Strait derived from CTD data. *Ocean Science*, *9*, 499–519. https://doi.org/10.5194/os-9-499-2013

Mauritzen, C. (1996). Production of dense overflow waters feeding the North Atlantic across the Greenland-Scotland Ridge. Part 1: Evidence for a revised circulation scheme. *Deep-Sea Research*, *43*(6), 769–806. https://doi.org/10.1016/0967-0637(96)00037-4

Melsheimer, C., & Spreen, G. (2019). *AMSR2 ASI sea ice concentration data, Arctic, version 5.4 (NetCDF) (July 2012–December 2018)*. PANGAEA. https://doi.org/10.1594/PANGAEA.898399

Melsheimer, C., & Spreen, G. (2020). *AMSR-E ASI sea ice concentration data, Arctic, version 5.4 (NetCDF) (June 2002–September 2011)*. PANGAEA. https://doi.org/10.1594/PANGAEA.919777

Nayar, K. G., Sharqawy, M. H., Banchik, L. D., & Lienhard, J. H. (2016). Thermophysical properties of seawarer: A review and new correlations that include pressure dependence. *Desalination*, *390*, 1–24. https://doi.org/10.1016/j.desal.2016.02.024

Quadfasel, D., Gascard, J.-C., & Koltermann, K.-P. (1987). Large-scale oceanography in Fram Strait during the 1984 marginal ice zone experiment. *Journal of Geophysical Research*, *92*(C7), 6719–6728. https://doi.org/10.1029/jc092ic07p06719

Richter, M. E., von Appen, W.-J., & Wekerle, C. (2018). Does the East Greenland Current exist in the northern Fram Strait? *Ocean Science*, *14*, 1147–1165. https://doi.org/10.5194/os-14-1147-2018

Ricker, R., Girard-Ardhuin, F., Krumpen, T., & Lique, C. (2018). Satellite-derived sea ice export and its impact on Arctic ice mass balance. *Cryosphere*, *12*, 3017–3032. https://doi.org/10.5194/tc-12-3017-2018

Rudels, B. (1987). *On the mass balance of the Polar Ocean, with special emphasis on the Fram Strait*. Norsk Polarinstitutt Skrifter, 188, 1–53. Retrieved from https://brage.npolar.no/npolar-xmlui/bitstream/handle/11250/173528/Skrifter188.pdf?sequence=1

Rudels, B., Björk, G., Nilsson, J., Winsor, P., Lake, I., & Nohr, C. (2005). The interaction between waters from the Arctic Ocean and the Nordic Seas north of Fram Strait and along the East Greenland Current: Results from the Arctic Ocean-02 Oden expedition. *Journal of Marine Systems*, *55*, 1–30. https://doi.org/10.1016/j.jmarsys.2004.06.008

Rudels, B., & Quadfasel, D. (1991). Convection and deep water formation in the Arctic Ocean - Greenland Sea System. *Journal of Marine Systems*, *2*, 435–450. https://doi.org/10.1016/0924-7963(91)90045-V

Schaffer, J., Timmermann, R., Arndt, J. E., Rosier, S. H. R., Aner, P. G. D., Callard, L. S., & Roberts, D. H. (2019). *An update to Greenland and Antarctic ice sheet topography, cavity geometry, and global bathymetry (RTopo-2.0.4)*. PANGAEA. https://doi.org/10.1594/PANGAEA.905295

Schaffer, J., Timmermann, R., Erik Arndt, J., Savstrup Kristensen, S., Mayer, C., Morlighem, M., & Steinhage, D. (2016). A global, high-resolution data set of ice sheet topography, cavity geometry, and ocean bathymetry. *Earth System Science Data*, *8*, 543–557. https://doi.org/10.5194/essd-8-543-2016

Schauer, U., Fahrbach, E., Osterhus, S., & Rohardt, G. (2004). Arctic warming through the Fram Strait: Oceanic heat transport from 3 years of measurements. *Journal of Geophysical Research*, *109*, C06026. https://doi.org/10.1029/2003JC001823

Schlichtholz, P., & Houssais, M. N. (1999). An inverse modeling study in Fram Strait. Part I: Dynamics and circulation. *Deep-Sea Research Part II*, *46*, 1083–1135. https://doi.org/10.1016/S0967-0645(99)00018-1

Sharqawy, M. H., Lienhard, VJ. H., & Zubair, S. M. (2010). Thermophysical properties of seawater: A review of existing correlations and data. *Desalination and Water Treatment*, *16*, 354–380. https://doi.org/10.5004/dwt.2010.1079

Smith, W. H., & Wessel, P. (1990). Gridding with continuous curvature splines in tension. *Geophysics*, *55*(3), 293–305. https://doi.org/10.1190/1.1442837

Spreen, G., Kaleschke, L., & Heygster, G. (2008). Sea ice remote sensing using AMSR-E 89-GHz channels. *Journal of Geophysical Research*, *113*, C02S03. https://doi.org/10.1029/2005JC003384

Trodahl, M., & Isachsen, P. E. (2018). Topographic influence on baroclinic instability and the mesoscale eddy field in the northern North Atlantic Ocean and the Nordic Seas. *Journal of Physical Oceanography*, *48*, 2593–2607. https://doi.org/10.1175/JPO-D-17-0220.1

Tsujino, H., Urakawa, S., Nakano, H., Small, R. J., Kim, W. M., Yeager, S. G., et al. (2018). JRA-55 based surface dataset for driving ocean-sea-ice models (JRA55-do). *Ocean Modelling*, *130*, 79–139. https://doi.org/10.1016/j.ocemod.2018.07.002

von Appen, W.-J. (2018). *The expedition PS114 of the research vessel POLARSTERN to the Fram Strait 2018*. Reports on Polar and Marine Research. https://doi.org/10.2312/BzPM_0723_2018

von Appen, W.-J. (2019). *Physical oceanography and current meter data (including raw data) from FRAM moorings in the Fram Strait 2016–2018*. PANGAEA. https://doi.org/10.1594/PANGAEA.904565

von Appen, W.-J., Beszczynska-Möller, A., Schauer, U., & Fahrbach, E. (2019). *Physical oceanography and current meter data from moorings F1-F14 and F15/F16 in the Fram Strait, 1997-2016*. PANGAEA. https://doi.org/10.1594/PANGAEA.900883

von Appen, W.-J., Schauer, U., Hattermann, T., & Beszczynska-Möller, A. (2016). Seasonal Cycle of Mesoscale Instability of the West Spitsbergen Current. *Journal of Physical Oceanography*, *46*, 1231–1254. https://doi.org/10.1175/jpo-d-15-0184.1

von Appen, W.-J., Wekerle, C., Hehemann, L., Schourup-Kristensen, V., Konrad, C., & Iversen, M. H. (2018). Observations of a submesoscale cyclonic filament in the marginal ice zone. *Geophysical Research Letters*, *45*, 6141–6149. https://doi.org/10.1029/2018GL077897

Wang, Q., Danilov, S., Sidorenko, D., Timmermann, R., Wekerle, C., Wang, X., et al. (2014). The Finite Element Sea Ice-Ocean Model (FESOM) v.1.4: Formulation of an ocean general circulation model. *Geoscientific Model Development*, *7*, 663–693. https://doi.org/10.5194/gmd-7-663-2014

Wekerle, C. (2021). FESOM model data used in the paper 'Seasonal and Mesoscale Variability of the Two Atlantic Water Recirculation Pathways in Fram Strait'. *Zenodo*. https://doi.org/10.5281/zenodo.4696124

Wekerle, C., Hattermann, T., Wang, Q., Crews, L., von Appen, W.-J., & Danilov, S. (2020). Properties and dynamics of mesoscale eddies in Fram Strait from a comparison between two high-resolution ocean–sea ice models. *Ocean Science*, *16*, 1225–1246. https://doi.org/10.5194/os-16-1225-2020

Wekerle, C., Wang, Q., von Appen, W.-J., Danilov, S., Schourup-Kristensen, V., & Jung, T. (2017). Eddy-resolving simulation of the Atlantic Water circulation in the Fram Strait with focus on the seasonal cycle. *Journal of Geophysical Research: Oceans*, *122*, 8385–8405. https://doi.org/10.1002/2017JC012974

Zhao, M., Timmermans, M.-L., Cole, S., Krishfield, R., Proshutinsky, A., & Toole, J. (2014). Characterizing the eddy field in the Arctic Ocean halocline. *Journal of Geophysical Research: Oceans*, *119*, 8800–8817. https://doi.org/10.1002/2014JC010488